Available online at www.sciencedirect.com
ScienceDirect
Journal of Sound and Vibration 308 (2007) 735–757
JOURNAL OF SOUND AND VIBRATION
www.elsevier.com/locate/jsvi

Nonlinear dynamic analysis of an elastic beam isolator sliding on frictional supports

R.A. Ibrahim*, R.J. Somnay

Department of Mechanical Engineering, Wayne State University, Detroit, MI 48202, USA

The peer review of this article was organised by the Guest Editor
Available online 8 June 2007

Abstract

The dynamic behavior of an elastic beam free to slide on two frictional supports is studied under sinusoidal and random excitations. The beam force–deflection relationship, originally expressed in terms of elliptic functions, is approximated by a polynomial fit of eleventh order. The friction force is modeled in terms of the sliding velocity and the end slope angle. Under sinusoidal excitation, the equation of motion of the system is solved numerically and the solution is utilized to estimate the system transmissibility. It is found that when the excitation frequency is increased beyond resonance, the friction at the sliding supports improves the transmissibility. The dependence of the response on initial conditions establishes the basins of attraction for different values of friction coefficient and excitation parameters. The dependence of the safety integrity factor on excitation amplitude level and friction coefficient reveals that the friction extends the stable region. Under random excitation, the system response statistics are estimated from Monte Carlo simulation results for different values of friction coefficient and excitation power spectral density level. The friction is found to result in a significant reduction of the system response mean square.
© 2007 Elsevier Ltd. All rights reserved.

1. Introduction

Linear vibration isolators are known to be effective if the value of their natural frequency is well below the excitation frequency. However, they are limited for such applications of moderate environmental disturbances, and under severe environmental disturbances such as shocks, impact loading, or ground random motion, their spectrum will definitely contain dangerous low frequencies components. The isolator under these conditions experiences excessive deflections that can cause over-stress and even damage to the system. The influence of isolator nonlinearity on its transmissibility depends on whether its stiffness is hard or soft [1]. It is known that soft nonlinearity causes a reduction in the resonant frequency and the isolation may be improved.

Nonlinearity becomes important in the study of an isolator when large deflections occur due to the effects of equipment weight and sustained acceleration. These effects are encountered in the behavior of suspensions of high-speed vehicles and mounts for sensitive instruments [2]. Many researchers have conducted studies

*Corresponding author.
E-mail address: ibrahim@eng.wayne.edu (R.A. Ibrahim).

0022-460X/$ - see front matter © 2007 Elsevier Ltd. All rights reserved.
doi:10.1016/j.jsv.2007.04.043

considering various combinations of restoring force and damping functions. Den Hartog [3] reported the exact solution for the vibratory response of a symmetric system with both coulomb and viscous damping when subjected to a harmonic forcing function. Ruzicka and Derby [4] presented extensive results for isolation systems with linear stiffness and nonlinear nth power damping. Hundal and Parnes [5] considered the same system when subjected to base excitation. Metwalli [6] proposed a model to optimize nonlinear suspension systems which approach optimal isolation characteristics. Optimized nonlinear isolator systems were found to outperform their linear counterparts.

The influence of nonlinearity on the performance of these isolators is manifested in shifting the resonance frequency and possibility of chaotic motion. Other factors include the type of excitation and its frequency spectrum. Depending on the type of nonlinearity, the resonance frequency may be shifted to the left or right of the linear resonance frequency on the transmissibility plot. Ravindra and Mallik [7] examined the response of nonlinear vibration isolation system subjected to force excitation or base excitation. It was found that an isolator with soft nonlinear characteristics is superior to the one with hard nonlinearity. The effects of damping on resonance transmissibility and the high-frequency attenuation rate of the transmissibility were found to be similar to those with a linear restoring force.

Note that in nonlinear isolators the transmitted signal may contain subharmonic, superharmonic, and sometimes chaotic behavior. Thus, the transmissibility defined by the linear theory of vibration isolation should be redefined by using a suitable performance index. Lou et al. [8] proposed the ratio of the rms values of the response amplitude to the excitation amplitude. This index provides a measure of the energy transmission relationship.

Under harmonic excitation, a nonlinear isolator may exhibit chaotic behavior over a certain range of system and excitation parameters. A simple method for describing the arbitrary multiaxial loading process of vibration isolation with large nonlinear stiffness and damping parameters was proposed by Ulanov and Lazutkin [9]. Qing et al. [10] treated the vibration isolation efficiency of nonlinear vibration–isolation system in a desired chaotic state. The transmitted force was characterized by a broad frequency band although the excitation was sinusoidal. In order to control the system in a desired chaotic state, the isolator had to possess variable stiffness and damping.

Systems subjected to impact and shock loads exhibit severe vibrations, and they need special isolation means. Impact loading is encountered in many mechanical applications such as pneumatic hammers, slamming loads on water waves acting on ships and ocean structures, and vibro-impact systems with rigid or elastic stops. In order to protect a given object against these undesirable disturbances, a vibrating protecting system is placed between the vibration source and the object. In their research monograph, Alabuzhev et al. [11] introduced a number of vibration protecting systems with quasi-zero stiffness whose load bearing elastic elements possess constant positive stiffness as well as devices with negative stiffness. This type of isolators has been used for vibration isolation of operators' seats in vehicles [12], impact action hand-held machines [13–15], and railway car suspensions [13,16]. Systems with negative stiffness have been treated by Gerner et al. [17] and Yuryev [18] and their performance in the chaotic regime was studied by Goverdovskiy et al. [19], Lee and Goverdovskiy [20], and Lee et al. [21].

Dufour et al. [22] recommended some modifications of the nonlinear characteristics of isolating mounts carrying rigid structures subjected to impact loads. The modifications were adapted with respect to impact vibrations to achieve a well design behavior. The protection of workers against vibrations generated from hand-held tools requires special vibration isolation means. Dobry and Brzezinski [23] developed strong elastic nonlinear isolator to minimize the interaction force between the tool and the handle. In an effort to prevent injuries from impact impulse loads, Balandin et al. [24] presented a review of research activities dealing with the limiting performance analysis of impact isolation systems. Zhiqing and Pilkey [25] conducted the limiting performance analysis to study the optimal shock and impact isolation of mechanical systems via wavelet transform.

A bumpered vibration protection arrangement of a gimbaled electro-optical device was developed by Veprik et al. [26]. The installation of bumpers with enlarged travel reduces the probability of accidental impacts and effectively reduces the excessive deflections. However, the presence of bumpers turns the vibration isolation arrangement into a potential strongly nonlinear vibro-impact system with unfavorable characteristics [27,28]. In an effort to eliminate these characteristics, Babitsky and Veprik [27] introduced the combination of

an undamped low-frequency vibration isolator and optimally damped bumpers installed with minimal free travel distance.

One of the basic requirements of vibration isolators is to reduce the system restoring force, which results in a reduction of the resonant frequency. Many techniques have been developed to reduce the isolator resonant frequency. These include the curved cantilever springs for gravitational wave applications [29,30] and the triangular pre-bent cantilever springs [31–35].

The so-called Euler spring column has been utilized as a vertical isolator. A major advantage of the Euler spring is that it stores negligible static energy below its working range thereby minimizing both the stored elastic energy density and the spring mass required to support the suspended test mass [36,37]. This feature makes Euler springs an excellent candidate as a vertical isolator. The buckled or pre-bent column with fixed ends was used as a vibration isolator and analyzed by Virgin and Davis [38] and Plaut et al. [39]. The column was modeled as an extensible elastica, which allows large displacements in equilibrium. It was found that for sufficiently low damping and sufficiently high column stiffness, the axial transmissibility curves exhibit an infinite number of peaks. Plaut et al. [40] considered another system consisting of two bars hinged together through a rotational spring and a rotational dashpot with one end subjected to axial excitation. The equation of motion of the system, involving nonlinear inertia and nonlinear parametric excitation, was found to possess no stable solution if the static axial load is greater than the critical load. Chaotic motions were found to occur for most of the frequencies over the range $\omega_n < \Omega < 2\omega_n$, where ω_n and are the natural and excitation frequencies, respectively.

Shoup [41] developed a nonlinear elastic suspension vibration isolator consisting of a pair of flexible strips, which are clamped in a semicircular shape with a block mass between them. If a load, P, is applied downward on the mass the upper strip deflects into a shape called the "*nodal elastica*", while the lower strip deforms into a shape known as the "*undulating elastica*." Note that the stress in the strips is caused by the combined effects of bending and simple tension or compression. The elastic springs are doubly clamped beams and possess a beam natural frequency apart from the suspension dynamics. However, elastica springs will not perform as desired when the frequency of suspension motion is near to the beam natural frequency. The results of large deflection of a flexible bar were utilized to evaluate the deformation of an elastic ring subjected to two opposite radial compressive loads. Later, Shoup and Simmonds [42] developed nonlinear suspension systems with adjustable stiffness rate.

In addition to the above described isolators, other types of nonlinear isolators have been assessed by Ibrahim [43] in an extensive review article. One of the most interesting systems includes what is referred to as Gospodnetic–Frisch-Fay beam mounted on three symmetrical frictionless knife-edged supports. The beam is not restrained from both sides and thus is considered as inextensible, and a closed form solution for its deflection curve was given in terms of elliptic functions. This beam can be used as a resilient isolator between the machinery and the base in marine vessels. The beam can also model a load carrying bearing for pressure pipelines against earthquake ground motion [44,45]. The dynamic characteristic of this beam and its efficacy as a nonlinear isolator was considered by Somnay et al. [46] under frictionless sliding supports. The present paper is an extension of Ref. [44] by including the influence of friction.

2. Analytical modeling

Fig. 1(a) shows an elastic beam free to slide at two knife-edged supports under the action of the load P. As the load increases both the beam length, L, and the end slope angle, ψ_0, increase simultaneously. d denotes the displacement at the mid-span, $x = l/2$, where l is the distance between the two supports A and B. Note that L and l are only equal when the beam is horizontal without any sag. The dependence of the beam deflection on the applied load was originally derived by Gospodnetic [47] and Frisch-Fay [48]. For frictionless supports, the deflection of the beam was written in terms of the slope angle ψ as

$$\frac{d\psi}{ds} = \frac{M}{EI} = \frac{P}{2EI}[(l/2 - x) + (d - y)\tan\psi_0], \tag{1}$$

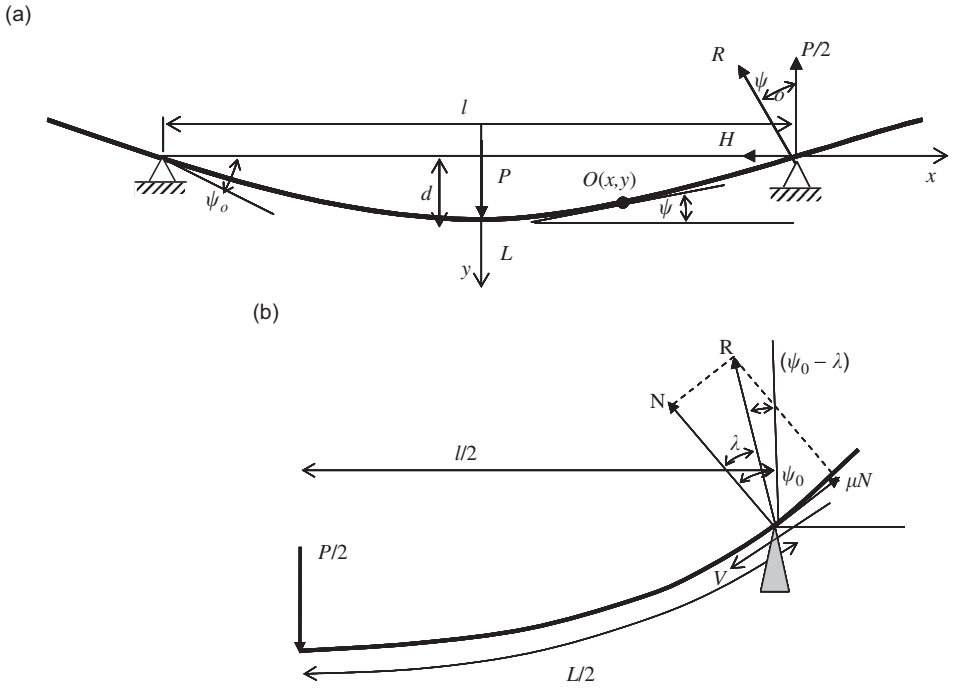

Fig. 1. Schematic diagram a flexible beam free to slide on (a) frictionless and (b) friction supports.

where M is the bending moment. Taking the derivative with respect to s, gives

$$\frac{\mathrm{d}^2\psi}{\mathrm{d}s^2} = -k^2\left[\frac{\mathrm{d}x}{\mathrm{d}s} + \frac{\mathrm{d}y}{\mathrm{d}s}\tan\,\psi_0\right], \tag{2}$$

where $k^2 = P/2EI$. Integrating both sides with respect to ψ, gives

$$\frac{1}{2}\left(\frac{\mathrm{d}\psi}{\mathrm{d}s}\right)^2 = -k^2[\sin\,\psi - \cos\,\psi\,\tan\,\psi_0] + C. \tag{3}$$

At $x = l/2$, the bending moment vanishes, i.e., $(\mathrm{d}\psi/\mathrm{d}s)_{\psi=\psi_0} = 0$, and thus $C = 0$. Accordingly, Eq. (3) can be written in the form

$$\frac{\mathrm{d}\psi}{\mathrm{d}s} = k\sqrt{2(\cos\,\psi\,\tan\,\psi_0 - \sin\,\psi)} = \sin\,\psi\frac{\mathrm{d}\psi}{\mathrm{d}y} = \cos\,\psi\frac{\mathrm{d}\psi}{\mathrm{d}x}. \tag{4}$$

From Eq. (4) it is possible to write

$$\mathrm{d}x = \cos\,\psi\,\mathrm{d}s = \cos\,\psi\frac{\mathrm{d}\psi}{k\left[2(\tan\,\psi_o\,\cos\,\psi - \sin\,\psi)\right]^{1/2}}, \tag{5}$$

$$\mathrm{d}y = \sin\,\psi\,\mathrm{d}s = \sin\,\psi\frac{\mathrm{d}\psi}{k\left[2(\tan\,\psi_o\,\cos\,\psi - \sin\,\psi)\right]^{1/2}}. \tag{6}$$

Introducing the transformation of variables $\cos\,\phi = \sqrt{\sin(\psi_o - \psi)}$ and $\cos\,\phi_o = \sqrt{\sin\,\psi_o}$, and integrating Eqs. (5) and (6) gives

$$l = \frac{2\sqrt{\cos\,\psi_o}}{k}\left(\sqrt{2}\cos\,\psi_o\,\cos\,\phi_o + \sin\,\psi_o\Phi\left(1\Big/\sqrt{2}, \phi_o\right)\right), \tag{7}$$

$$y = d = \frac{\sqrt{\cos\psi_o}}{k}\left(\sqrt{2}\sin\psi_o\cos\phi_o - \cos\psi\Phi\left(1\Big/\sqrt{2},\phi_o\right)\right), \tag{8}$$

where

$$\begin{aligned}\Phi(\phi_o) &= F\left(1\Big/\sqrt{2},\phi_o\right) - K\left(1\Big/\sqrt{2}\right) + 2E\left(1\Big/\sqrt{2}\right) - 2E\left(1\Big/\sqrt{2},\phi_o\right)\\ &= 0.8472 + F\left(1\Big/\sqrt{2},\phi_o\right) - 2E\left(1\Big/\sqrt{2},\phi_o\right)\end{aligned}$$

and $F(1/\sqrt{2},\phi_o)$, $E(1/\sqrt{2},\phi_o)$, $K(1/\sqrt{2})$ and $E(1/\sqrt{2})$ are the incomplete integral of the first kind, the incomplete integral of the second kind, the complete integral of the first kind and the complete integral of the second kind, respectively.

Eqs. (7) and (8) may also be written in the form (Somnay et al. [46])

$$\frac{Pl^2}{EI} = 8\cos\psi_o\left(\sqrt{2}\cos\psi_o\cos\phi_o + \sin\psi_o\Phi\left(1\Big/\sqrt{2},\phi_o\right)\right)^2, \tag{9}$$

$$\frac{d}{l} = \frac{1}{2}\frac{\sqrt{2}\sin\psi_o\cos\phi_o - \cos\psi_o\Phi\left(1/\sqrt{2},\phi_o\right)}{\sqrt{2}\cos\psi_o\cos\phi_o + \sin\psi_o\Phi\left(1/\sqrt{2},\phi_o\right)}. \tag{10}$$

If friction at the supports is considered, the reaction at the supports consists of normal and tangential components, as shown in Fig. 1(b). The support reaction, R, is inclined at an angle $(\psi_o-\lambda)$ to the vertical, where $\mu = \tan\lambda = F_f/N$, is the coefficient of friction. The vertical component of the reaction R must balance $P/2$, hence

$$R = \frac{P}{2\cos(\psi_o - \lambda)}. \tag{11}$$

The equations developed in the frictionless model can be used again by replacing ψ_o by $(\psi_o-\lambda)$. Eqs. (9) and (10) with the appropriate substitution are

$$\frac{Pl^2}{EI} = 8\cos(\psi_o-\lambda)\left(\sqrt{2}\cos(\psi_o-\lambda)\cos\phi_o + \sin(\psi_o-\lambda)\Phi(p,\phi_o)\right), \tag{12}$$

$$\frac{d}{l} = \frac{1}{2}\left(\frac{\sqrt{2}\sin(\psi_o-\lambda)\cos\phi_o - \cos(\psi_o-\lambda)\Phi(p,\phi_o)}{\sqrt{2}\cos(\psi_o-\lambda)\cos\phi_o + \sin(\psi_o-\lambda)\Phi(p,\phi_o)}\right). \tag{13}$$

The force–deflection relationship is approximated as best-fit polynomial of the form

$$\frac{Pl^2}{EI} = a_1\left(\frac{d}{l}\right) + a_3\left(\frac{d}{l}\right)^3 + a_5\left(\frac{d}{l}\right)^5 + a_7\left(\frac{d}{l}\right)^7 + a_9\left(\frac{d}{l}\right)^9 + a_{11}\left(\frac{d}{l}\right)^{11}, \tag{14}$$

where the coefficients a_1 through a_{11} are the coefficients of the best-fit polynomial, and giving by the values: $a_1 = 48.0$, $a_3 = -402.0$, $a_5 = 1670.6$, $a_7 = -3749.0$, $a_9 = 4256.4$, $a_{11} = -1903.5$.

Fig. 2 shows the dependence of the beam deflection on the applied load for three values of friction coefficient, $\mu = 0.0, 0.1, 0.2$. It is seen that as the friction at the support increases the peak load and deflection increase as well.

The sliding velocity, V, defines the direction of the friction force. The friction–velocity relationship may be modeled as a continuous transcendental function [49]:

$$\mu\,\mathrm{sgn}(V) \cong [\mu_k + (\mu_s - \mu_k)/\cosh(\beta V)]\tanh(\alpha V), \tag{15}$$

where μ_s and μ_k are the static and kinetic friction coefficients. α and β are parameters governing the friction curve slope at zero sliding velocity. Eq. (15) reveals that the friction at zero velocity is a smooth curve and avoids the jump discontinuity. This smoothens eliminates the mathematical difficulties encountered in the problem of differential inclusion [50].

Eq. (15) requires a kinematical relationship between the relative sliding velocity at the support and the velocity at the beam center. The sliding velocity is given by the time derivative of the total length of the beam

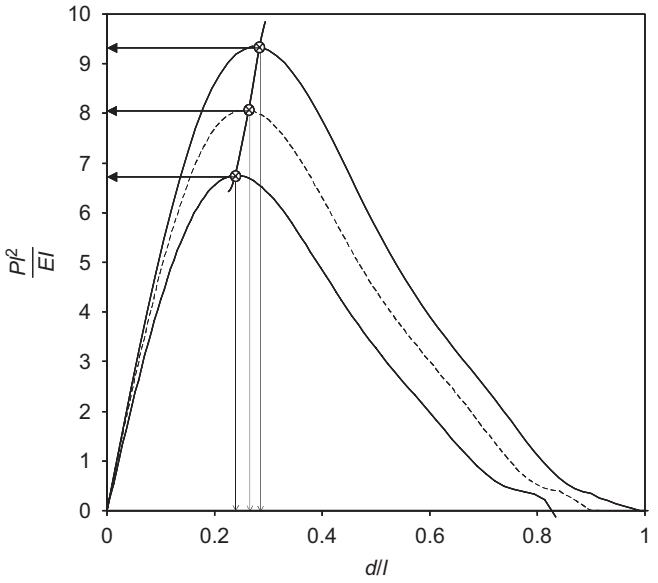

Fig. 2. Load deflection curve showing increase in critical stable load due to friction ⊗. ····· frictionless supports $\mu = 0.0$; -------- $\mu = 0.1$; _____ $\mu = 0.2$.

L, which is changing as the beam undergoes deflection. The total length is given by

$$L = 2\int_0^{\psi_o} \mathrm{d}s = 2\int_o^{\psi_o} \frac{\mathrm{d}s}{\mathrm{d}\psi}\,\mathrm{d}\psi = 2\int_0^{\psi_o} \frac{\mathrm{d}\psi}{k[2\tan\psi_o\cos\psi - \sin\psi]^{1/2}}$$
$$= \frac{\sqrt{\cos\psi_o}}{k}\left[K\left(1\Big/\sqrt{2}\right) - F\left(1\Big/\sqrt{2}, \phi_o\right)\right]. \tag{16}$$

The length of the sliding beam is a function of the end slope angle, ψ_o, which in turn is a function of the beam center deflection, d as given by Eqs. (12) and (13). Thus, Eq. (16) relates the beam sliding length L to the center deflection. For the purpose of the present analysis, it is convenient to express Eq. (16) as a polynomial function which is obtained by curve fitting. The best-fit polynomial function is expressed as

$$\frac{L}{l} = 1 + l_1\left(\frac{d}{l}\right)^2, \tag{17}$$

where $l_1 = 2.2092$. The sliding velocity at the support can be obtained by differentiating Eq. (17) and replacing the deflection as a non-dimensional variable:

$$\bar{V} = \tfrac{1}{2}\dot{\tilde{L}} = l_1\tilde{d}\dot{\tilde{d}}. \tag{18}$$

The end slope angle, ψ_o, is expressed as a function of center displacement and the curve fit approximation of this relationship is

$$\psi_0 = s_1\frac{d}{l} = s_1\tilde{d}. \tag{19}$$

The constant $s_1 = 2.757$ when the end slope angle is expressed in radians.

To simplify the dynamic modeling the mass of beam is neglected and the static load is only due to the weight of the carried machine of mass, m, that produces sinusoidal dynamic unbalance force, $F(t) = F_0\sin\Omega t$, where F_0 and Ω are the excitation amplitude and frequency, respectively. The total potential energy, PE, is the sum of

gravitational potential energy and elastic potential energy

$$\mathrm{PE} = \frac{EId^2}{l^3}\left(\frac{a_1}{2} + \frac{a_3}{4}\left(\frac{d}{l}\right)^2 + \frac{a_5}{6}\left(\frac{d}{l}\right)^4 + \frac{a_7}{8}\left(\frac{d}{l}\right)^6 + \frac{a_9}{10}\left(\frac{d}{l}\right)^4 + \frac{a_{11}}{12}\left(\frac{d}{l}\right)^{10}\right) - mgd. \tag{20}$$

The kinetic energy of the system is given by

$$\mathrm{KE} = \tfrac{1}{2}m\dot{d}^2. \tag{21}$$

The externally applied excitation force and the vertical component of the friction force are

$$\begin{aligned} Q_k &= F_o \sin \Omega t + mg - 2\mu \,\mathrm{sgn}(\bar{V})N \sin \psi_o \\ &= F_o \sin \Omega t + mg - \frac{\mu \,\mathrm{sgn}(\bar{V})(F(t) + mg)\cos \lambda \sin \psi_o}{\cos(\psi_o - \lambda)}. \end{aligned} \tag{22}$$

The function $\mathrm{sgn}(\bar{V})$ is used to specify the sign for the friction force as being opposed to the sliding velocity $\bar{V}$. For brevity, we introduce the friction function $F_f(\psi_o, \lambda)$ as

$$F_f(\psi_0, \lambda) = \frac{\mu \,\mathrm{sgn}(\bar{V})\cos \lambda \sin \psi_0}{\cos(\psi_0 - \lambda)}. \tag{23}$$

Substituting Eqs. (20)–(22) into Lagrange's equation gives the equation of motion for the isolator as

$$\begin{aligned} &m\ddot{d} + \frac{EIa_1}{l^3}d + \frac{EIa_3}{l^5}d^3 + \frac{EIa_5}{l^7}d^5 + \frac{EIa_7}{l^9}d^7 + \frac{EIa_9}{l^{11}}d^9 + \frac{EIa_{11}}{l^{13}}d^{11} \\ &\quad = \left[(F_o \sin \Omega t + mg)(1 - F_f(\psi_o, \lambda))\right]. \end{aligned} \tag{24}$$

For the development of the dynamic equation of motion it is necessary to modify Eq. (24) such that the response displacement is measured from the static equilibrium position. This is done by defining the vibratory or perturbation component of the deflection as $y = d - S$, where S, is the static deflection and d is the total deflection. The static component is obtained from the static equilibrium equation:

$$a_1 S + \frac{a_3}{l^2}S^3 + \frac{a_5}{l^4}S^5 + \frac{a_7}{l^6}S^7 + \frac{a_9}{l^8}S^9 + \frac{a_{11}}{l^{10}}S^{11} = mg\frac{l^3}{EI}\left(1 - \frac{\mu \cos \lambda \sin \psi_o}{\cos(\psi_o - \lambda)}\right). \tag{25}$$

Substituting for $y = d - S$, and Eq. (25) into Eq. (24) gives the equation of motion in terms of the dynamic displacement, y. Introducing the non-dimensional variables $\tilde{y} = y/l$, $\tilde{S} = S/l$, $\tau = \omega_n t$, $f_o = F_0/(ml\omega_n^2)$, and $v = \Omega/\omega_n$, and adding viscous damping with damping factor, ζ, Eq. (24) takes the form

$$\begin{aligned} &\ddot{\tilde{y}} + 2\zeta\dot{\tilde{y}} + \tilde{y} + c_2\tilde{y}^2 + c_3\tilde{y}^3 + c_4\tilde{y}^4 + c_5\tilde{y}^5 + c_6\tilde{y}^6 + c_7\tilde{y}^7 + c_8\tilde{y}^8 + c_9\tilde{y}^9 + c_{10}\tilde{y}^{10} + c_{11}\tilde{y}^{11} \\ &\quad = f_o \sin v\tau\{1 - F_f(\psi_o\lambda)\}, \end{aligned} \tag{26}$$

where

$$\omega_n = \left\{\frac{EI}{ml^3}\left[a_1 + 3a_3\tilde{S}^2 + 5a_5\tilde{S}^4 + 7a_7\tilde{S}^6 + 9a_9\tilde{S}^8 + 11a_{11}\tilde{S}^{10}\right]\right\}^{1/2}$$

is the linear natural frequency of the beam, and the coefficients, c_i are given in Appendix A.

Substituting the kinematical relationships for $\bar{V}$ and ψ_o as given by Eqs. (18) and (19) into the expression for F_f Eq. (24) allows us to express F_f as a function of the central deflection d as

$$F_f(\psi_0, \bar{V}, \lambda) = F_f(d, \bar{V}, \lambda) = \frac{\mu \,\mathrm{sgn}(\bar{V})\cos \lambda \sin(s_1 d)}{\cos[(s_1 d) - \lambda]}. \tag{27}$$

The equation of motion (26) describes the dynamics of the beam including the friction at the two supports. It will be numerically solved to evaluate the steady-state response to a harmonic excitation in Sections 3 and 4. In Section 5, we will consider the random excitation of the beam. To this end, one should recall some important features of the unperturbed frictionless system with zero damping. The Hamiltonian of such system $H = \mathrm{KE} + \mathrm{PE}$, of this system and thus one can write the first integral of motion $\dot{y}^2 = 2[H - \mathrm{PE}(y)]$. As long as

$H > \mathrm{PE}(y)$ the phase diagram is periodic closed orbit in the phase space $\{y, \dot{y}\}$. It was indicated in Ref. [46] that H reaches its maximum value $H_{\max} = \mathrm{PE}(y_{\max}) = 0.02365$, where $y_{\max}$ is the maximum beam displacement when its restoring force vanishes. The periodic orbits are only restricted inside the domain $D = \{(y, \dot{y}) | H \leqslant H_c\}$, where $H_c = H_{\max} - \Delta H$, and ΔH is sufficiently small. H_c is the critical energy level above which collapse of the beam will take place, and the trajectories of the motion will be structurally unstable. The motion corresponding to $H_{\max} = 0.02365$ follows a homoclinic orbit with one saddle point on one side of the static equilibrium position similar to the cases of a biased ship in roll oscillation [46].

3. Steady-state response

The dependence of the friction force on the velocity in the vicinity of zero sliding velocity is characterized by a steep gradient. This feature makes the equation of motion belongs to a 'stiff' system in the numerical integration. Beginning with prescribed initial conditions, the solver steps through the time interval, computes a solution at each time step using a user supplied subroutine, which evaluates the force function together with its derivative. The solution for a given time step is converged if it satisfies the user specified error tolerance criterion, which is taken as 10^{-6}. If the out of balance force is greater than this tolerance the solver shrinks the step size and tries again. By far the most commonly used method of predicting the solution for the forward time step t_{n+1} based on the converged solution for the present time step t_n is the fourth-order Runge–Kutta method, which requires four evaluations on the right-hand side per step. The forward time step predictions are augmented using the special formulas (see, e.g., Ref. [51]), which have been shown to enhance the efficiency and accuracy of the numerical solution for moderately stiff problems such as the one encountered for the frictional vibrating beam.

The equation of motion for the frictional isolator (26) is reproduced here after dropping the over-tilde notation and transposing the frictional force term F_f to the left hand side:

$$\ddot{y} + 2\zeta\dot{y} + (f_o \sin v\tau) F_f(\psi_o, \bar{V}, \lambda) + y + c_2 y^2 + c_3 y^3 + c_4 y^4 + c_5 y^5 + c_6 y^6 + c_7 y^7 + c_8 y^8 + c_9 y^9 + c_{10} y^{10} + c_{11} y^{11} = f_o \sin v\tau. \tag{28}$$

Here, $F_f(\psi_o, \bar{V}, \lambda) F_f(\psi_o, \lambda)$ is the friction force at the support along the direction of motion, and is given by Eq. (27)

$$F_f(\psi_0, \bar{V}, \lambda) = \frac{\mu \,\mathrm{sgn}(\bar{V}) \cos\lambda \sin\psi_0}{\cos(\psi_0 - \lambda)}, \tag{29}$$

where λ is the friction angle. The expression for the total transmitted force F_t at the support is

$$F_t = \sqrt{F_{\mathrm{te}}^2 + (F_{\mathrm{td}} + F_{\mathrm{tf}})^2}, \tag{30}$$

where F_{te}, F_{td} and F_{tf} are the transmitted elastic, damping and friction forces, respectively. Using the absolute magnitudes of the terms in Eq. (29) the friction force component F_{tf} will be

$$F_{\mathrm{tf}} = \frac{f_o \mu \cos\lambda \sin(s_1 a)}{\cos(s_1 a - \lambda)}. \tag{31}$$

Here, a is the displacement amplitude obtained from the numerical simulation and $s_1 = 2.757$ is the curve fit coefficient of the end slope deflection equation. Incorporating Eqs. (30) and (31) into the definition of the transmissibility gives

$$\mathrm{TR}_{\mathrm{fr}} = \frac{F_t}{f_o} = \frac{a}{f_o}\sqrt{\left|1 + \frac{3}{4}c_3 a^2 + \frac{5}{8}c_5 a^4 + \frac{35}{64}c_7 a^6 + \frac{63}{128}c_9 a^8 + \frac{231}{512}c_{11} a^{10}\right|^2 + \left|2\zeta v + \frac{f_o \mu \cos\lambda \sin(s_1 a)}{a \cos(s_1 a - \lambda)}\right|^2}. \tag{32}$$

Fig. 3 shows the transmissibility plots of linear and nonlinear isolators with frictionless supports and frictional supports ($\mu_s = 0.5$ and $\mu_k = 0.3$). It is seen that the transmissibility of the frictional isolator in the

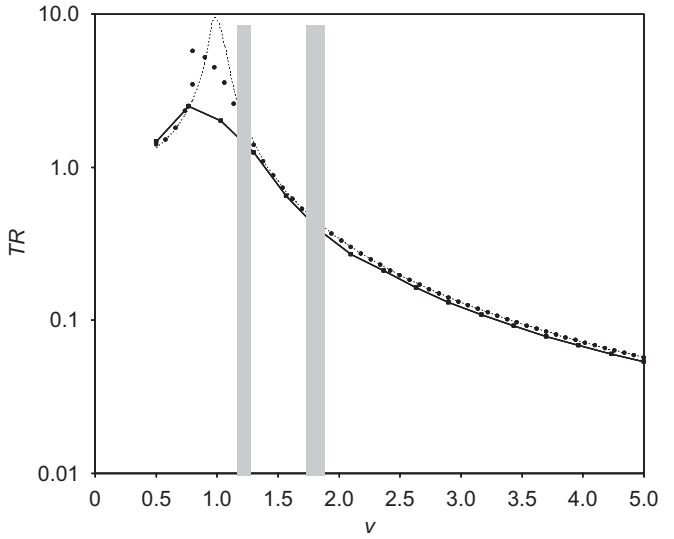

Fig. 3. Comparison of the transmissibility of • • • • linear isolator; ●●●●●: nonlinear isolator without friction; –■–■–■–■– nonlinear isolator with friction $\mu_s = 0.5$, $\mu_k = 0.3$.

low-frequency regime is improved when compared with the frictionless isolator and is superior to the linear one. When the excitation frequency is increased beyond resonance, the friction at the sliding support serves to improve the transmissibility when compared with the linear isolator. This improvement is attributed to the reduction in the amplitude of vibration that is a result of the opposing friction force.

The friction also introduces regimes where there is multiperiodic response. These are indicated by the shaded gray regions in Fig. 3. A segment of the response time history record over a non-dimensional time window of 50 units, corresponding phase portrait and FFT are shown in Figs. 4(a)–(c). Fig. 4 is generated under excitation frequency ratio $v = 1.22$ and amplitude $f_o = 0.025$. It is seen that due the asymmetry about the time axis, the response possesses non-zero mean, which is reflected in the FFT at zero frequency. The side frequencies that appear at the excitation frequency ratio $v = 1.22$ are attributed to the inherent nonlinearity of the isolator. Under excitation frequency ratio $v = 1.94$, the response dynamic characteristics are shifted to mono-periodic non-harmonic oscillations as shown in Figs. 5(a)–(c). Under an increased excitation amplitude of $f_o = 0.04$ there is a period doubling response at the low excitation frequency $v = 0.5$ as shown in the time histories and phase plots of Figs. 6(a)–(c). Figs. 7 and 8 show another two sets of response characteristics at two different values of excitation frequency ratio $v = 2.1$ and 2.3667, respectively, and same excitation level, $f_o = 0.04$. The response shown in Fig. 7 is mono-periodic while Fig. 8 exhibits period doubling. Note that these plots are generated for the same set of initial conditions. For different initial conditions the response characteristics may differ mainly due to the system inherent nonlinearity. This will be examined in the next section.

4. Basins of attraction

The dependence of the response on the initial conditions establishes the basins of attraction for different response characteristics. Figs. 9(a)–(f) show how the basins of attraction are affected by the value of the friction coefficient as it increases from $\mu_k = 0.0$ to 0.3. It is seen that the friction at the support restrains the beam and limits its deflection to a lower level than the point of instability. In the limiting case when the friction is infinitely large any sliding at the support will be prevented and the beam would be constrained to a fixed length. This would physically resemble a beam on simple supports, which is stable for all sets of initial conditions over the entire phase plane.

Throughout this study the frictional isolator response shows a strong dependence on initial conditions. For example, Figs. 10(a)–(c) show three response time history records for different initial conditions each

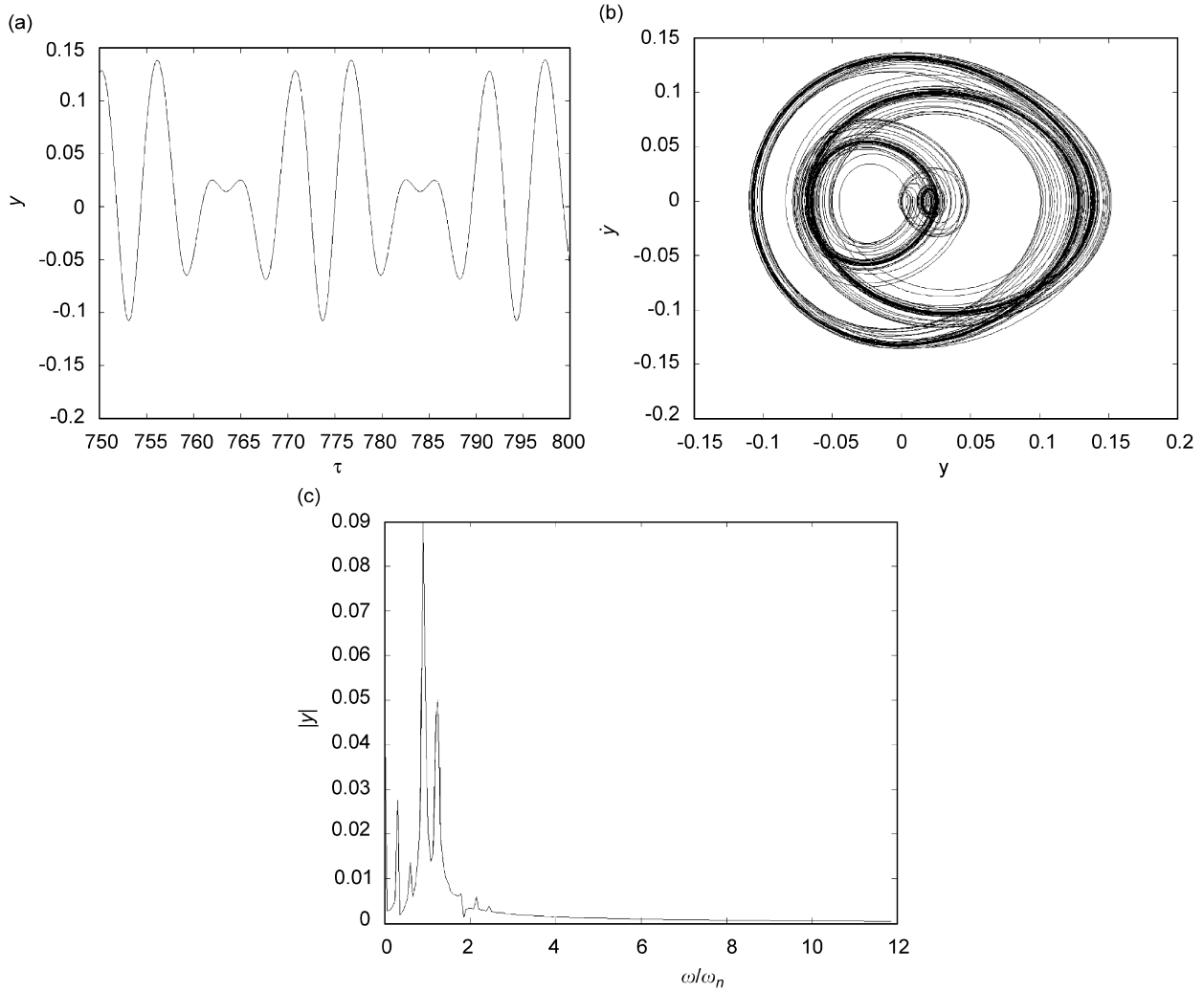

Fig. 4. (a) Response time history segment over 50 time unit window of frictional isolator showing multi-periodic non-harmonic response at excitation frequency $v = 1.22$ and $f_o = 0.025$, $\mu_s = 0.5$ and $\mu_k = 0.3$, and (b) phase portrait, and (c) FFT plot.

estimated for the same friction coefficient $\mu_k = 0.3$ and excitation parameters $v = 0.85$ and $f_o = 0.0329$. Note that Fig. 10(a) reveals a typical stable non-harmonic periodic response for the initial conditions $y(0) = -0.015$; $\dot{y}(0) = -0.1936$. The response exhibits multiperiodic characteristics for other set of initial conditions $y(0) = -0.106$; $\dot{y}(0) = 0.1584$ as indicated in Fig. 10(b). For another set of initial conditions $y(0) = -0.04$; $\dot{y}(0) = -0.1848$ the response becomes unstable as shown in Fig. 10(c).

Fig. 11 shows the dependence of the friction coefficient on the relative velocity for three different values of the kinetic friction coefficient according to Eq. (15). The dashed–solid point curve defines the locus of the friction peak where the slope of each curve is zero and any further increase in the sliding velocity produces a negative slope. This figure will help in better understanding the safety integrity factor that describes the safety regions of safe basins. The safety integrity factor (also referred to as the stability fraction) S_f is defined as the ratio of the area of the stable region in the phase plane (area of the safe basin) to the total area encompassed by the homoclinic orbit (of the unperturbed frictionless undamped system). S_f is evaluated for different levels of excitation parameters. Fig. 12 shows the dependence of the safety integrity factor on the excitation amplitude level for the three different values of friction coefficient ($\mu_k = 0.1$, 0.2, and 0.3) in addition to the zero friction case (indicated by the solid curve). All three curves show the tendency of the friction to prolong

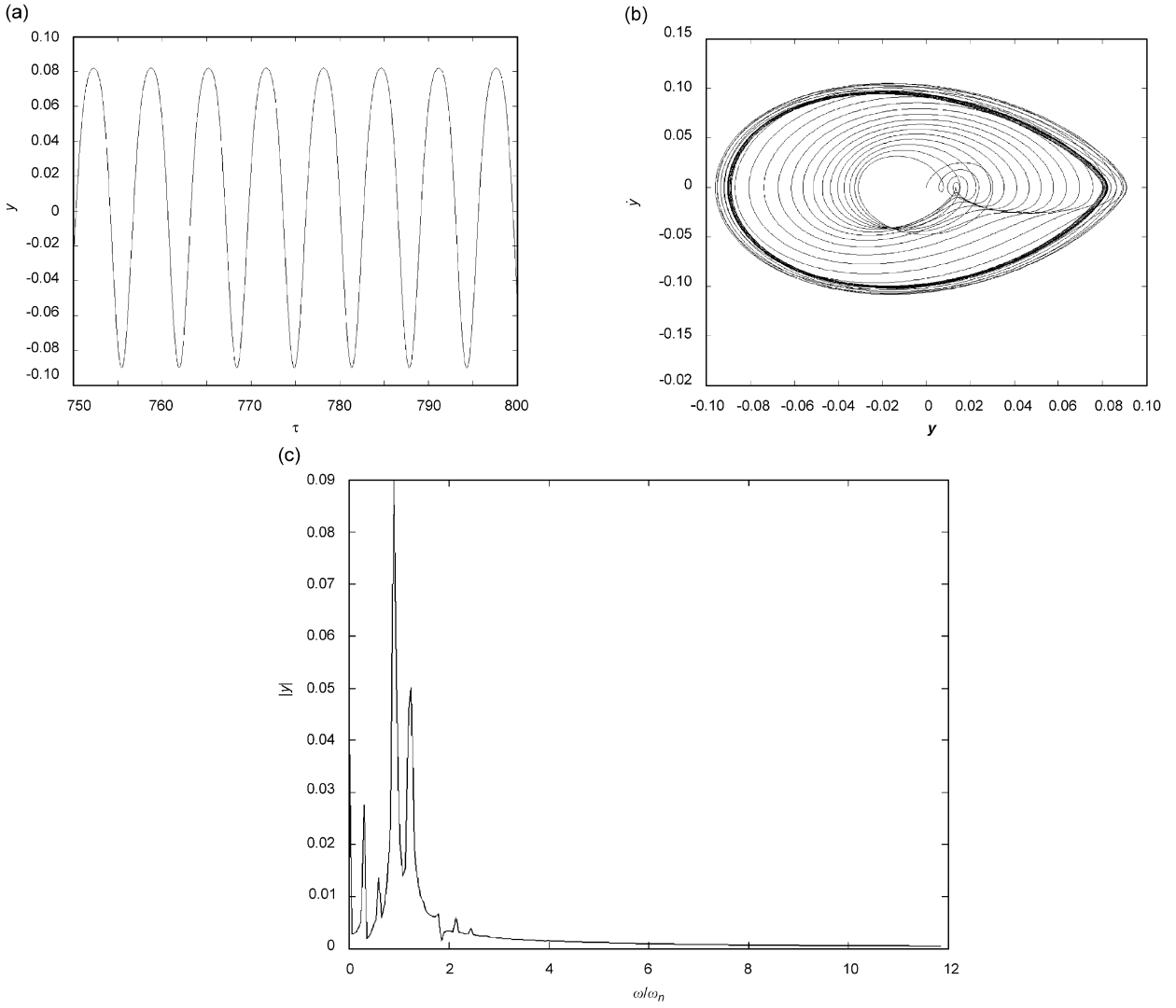

Fig. 5. (a) Response time history segment over 50 time unit window of frictional isolator showing multi-periodic non-harmonic response at excitation frequency $\nu = 1.94$ and $f_o = 0.025$ $\mu_s = 0.5$ and $\mu_k = 0.3$, and (b) phase portrait, and (c) FFT plot.

the stable region as reflected in the longer plateau, where S_f stays just under 1.0. However, it is observed that beyond a critical value of the excitation amplitude f_o, the curve drops off sharply. The points where the frictional curve intersects with the zero friction curve indicates a transition where the sliding friction at the supports is no longer beneficial in stabilizing the beam vibration. These points are marked as solid circles in Fig. 11. A closer examination of the state variables at these points indicates that the velocity amplitude under the corresponding excitation force reaches the critical values identified in Fig. 11 where the slope of the friction–velocity curve turns negative.

5. Random excitation of the isolator

The study described in the previous sections clearly indicates strong nonlinear characteristics of the isolator response. The problem becomes more complex when it comes to evaluating its response to random excitation. The system complexity arises from the nonlinear stiffness terms in addition to the support friction force. Several techniques have been developed to treat nonlinear systems subjected to random excitations. These

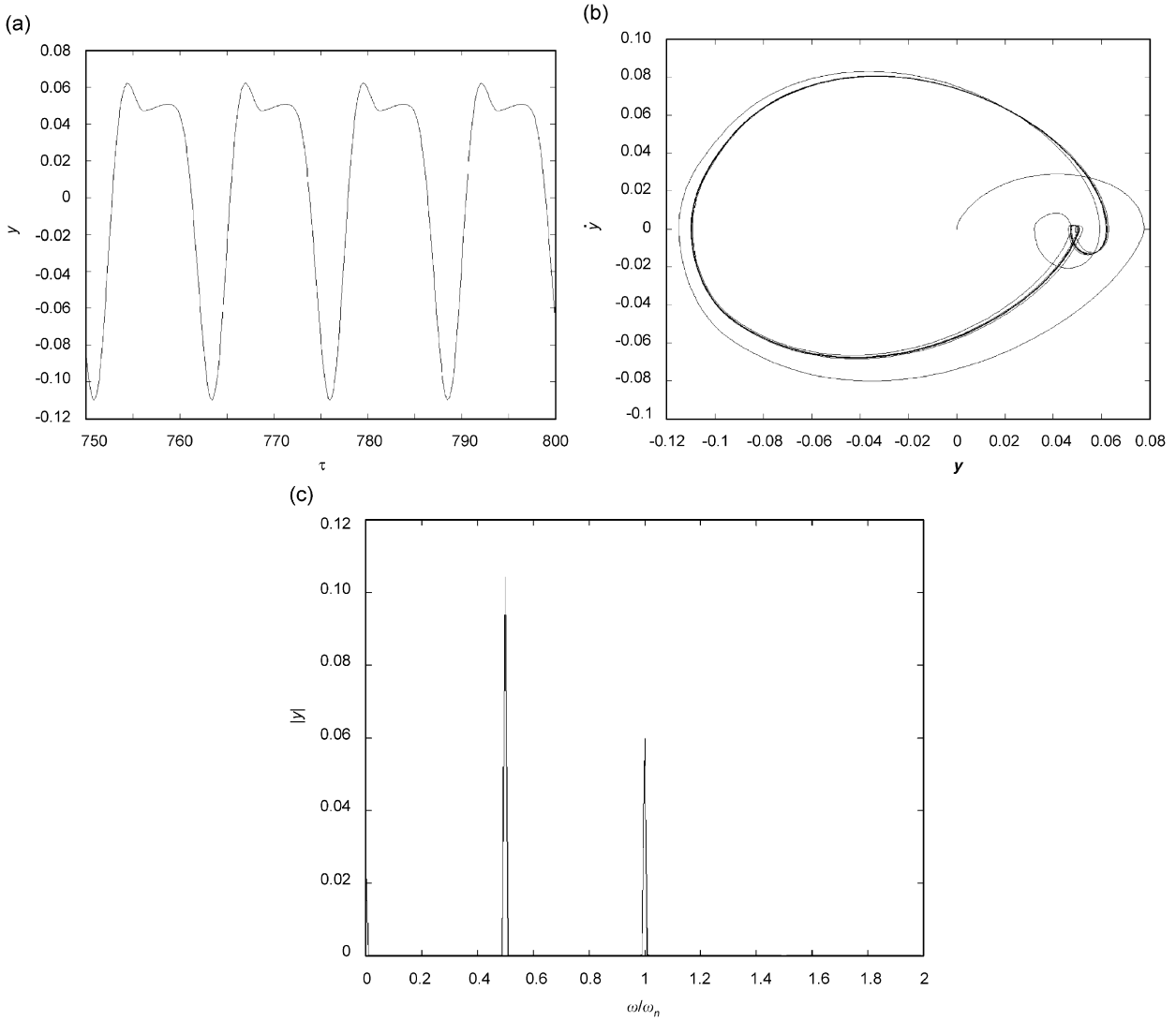

Fig. 6. (a) Response time history segment over 50 time unit window of frictional isolator showing multi-periodic non-harmonic response at excitation frequency $v = 0.5$ and $f_o = 0.04$ and $\mu_s = 0.5$ and $\mu_k = 0.3$, (b) phase portrait, and (c) FFT plot.

techniques include (1) stochastic averaging methods, (2) Ito Stochastic Calculus and Markov methods based on the Fokker–Planck equation, (3) perturbation techniques, (4) Gaussian and non-Gaussian closure schemes, (5) equivalent discretization method, and (6) Monte Carlo simulation. These approaches have been applied to dynamic systems with various forms of nonlinearities. However, there is no general rule about the suitability of any method for a particular given problem. When the excitation is modeled by a white noise process, the response of the system constitutes a Markov process and the response transition probability density function (pdf) is governed by the Fokker–Planck–Kolmogorov (FPK) equation. The solution of the stationary FPK equation has been obtained for the frictionless system in a closed form [46]. However, in the presence of friction it is difficult to solve for the corresponding FPK equation. Monte Carlo simulation is widely used for simulating the behavior of various physical and mathematical systems. It is distinguished from other numerical simulation methods due to the fact it utilizes random numbers for generating the random excitation. Because of the repetition of the algorithm and the large number of calculations involved, the Monte Carlo simulation requires considerable computing resources.

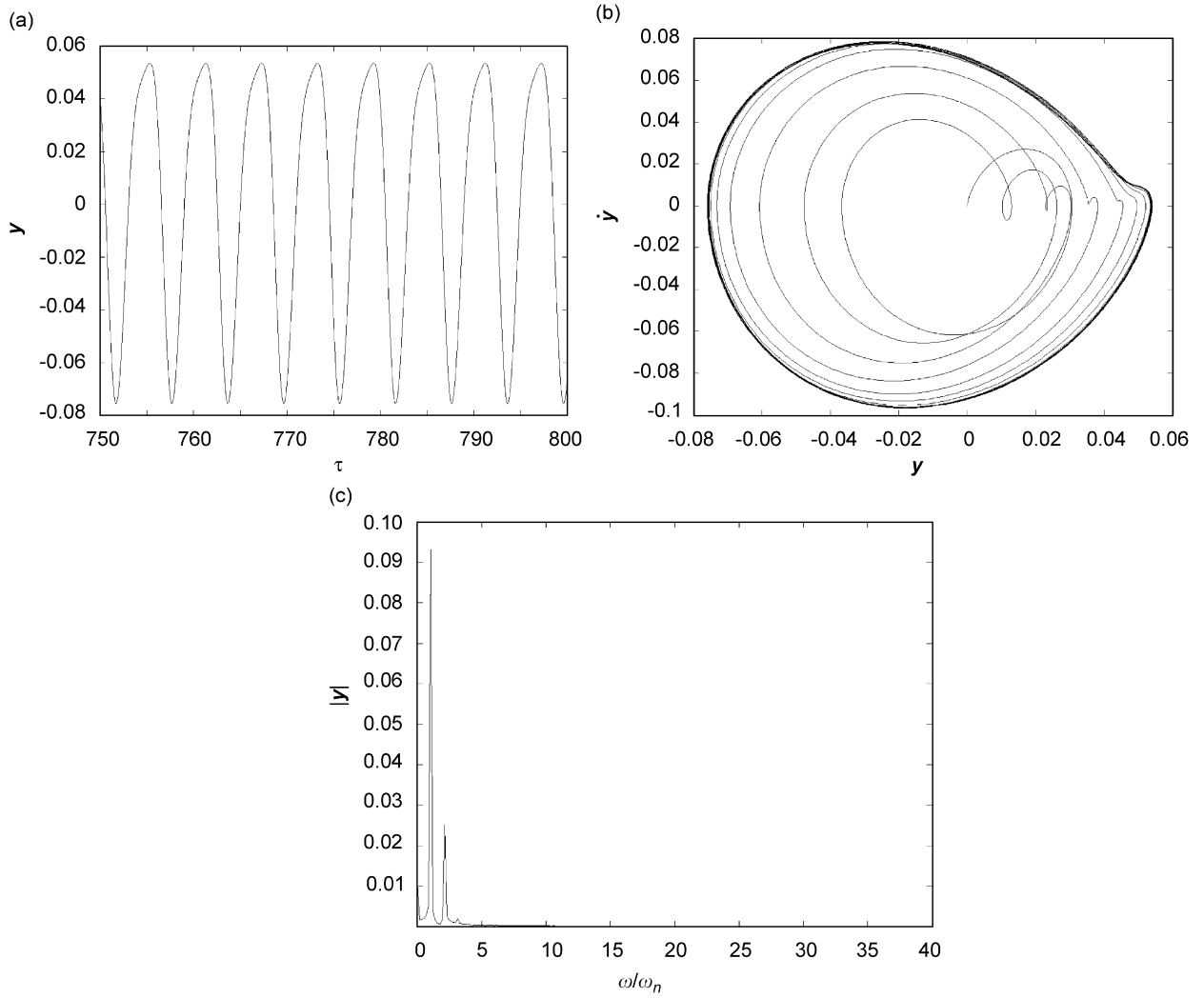

Fig. 7. (a) Response time history segment over 50 time unit window of frictional isolator showing multi-periodic non-harmonic response at excitation frequency $v = 2.1$ and $f_o = 0.04$ and $\mu_s = 0.5$ and $\mu_k = 0.3$, (b) phase portrait, and (c) FFT plot.

The equation of motion which defines the response of the flexible beam isolator subjected to a white noise excitation $W(\tau)$ takes the form

$$\ddot{y} + 2\zeta\dot{y} + y + c_2y^2 + c_3y^3 + c_4y^4 + c_5y^5 + c_6y^6 + c_7y^7 + c_8y^8 + c_9y^9 + c_{10}y^{10} + c_{11}y^{11} = W(\tau)(1 - F_f(\psi_o, \lambda)). \quad (33)$$

The suitable number of time records which numerically simulate the white noise excitation $W(\tau)$ is crucial to the successful implementation of this method. In this study, the MATLAB subroutine *RANDN* is selected to generate a sequence of Gaussian distributed random numbers using Marsaglia's Ziggurat algorithm [52]. These numbers are used to form the excitation time record by assigning them to the excitation force at successive time intervals. By controlling the value of the correlation time to the value $\Delta\tau = 0.01$ the excitation approaches a wide band random process. The power spectral density (PSD) function of the input excitation is evaluated for each excitation record to verify that it is a constant value over a wide frequency band.

The time integration of Eq. (33) for the specific excitation record is followed by evaluating the response statistics in the time, frequency and amplitude domains. In the time domain the mean $E[y]$ and mean square

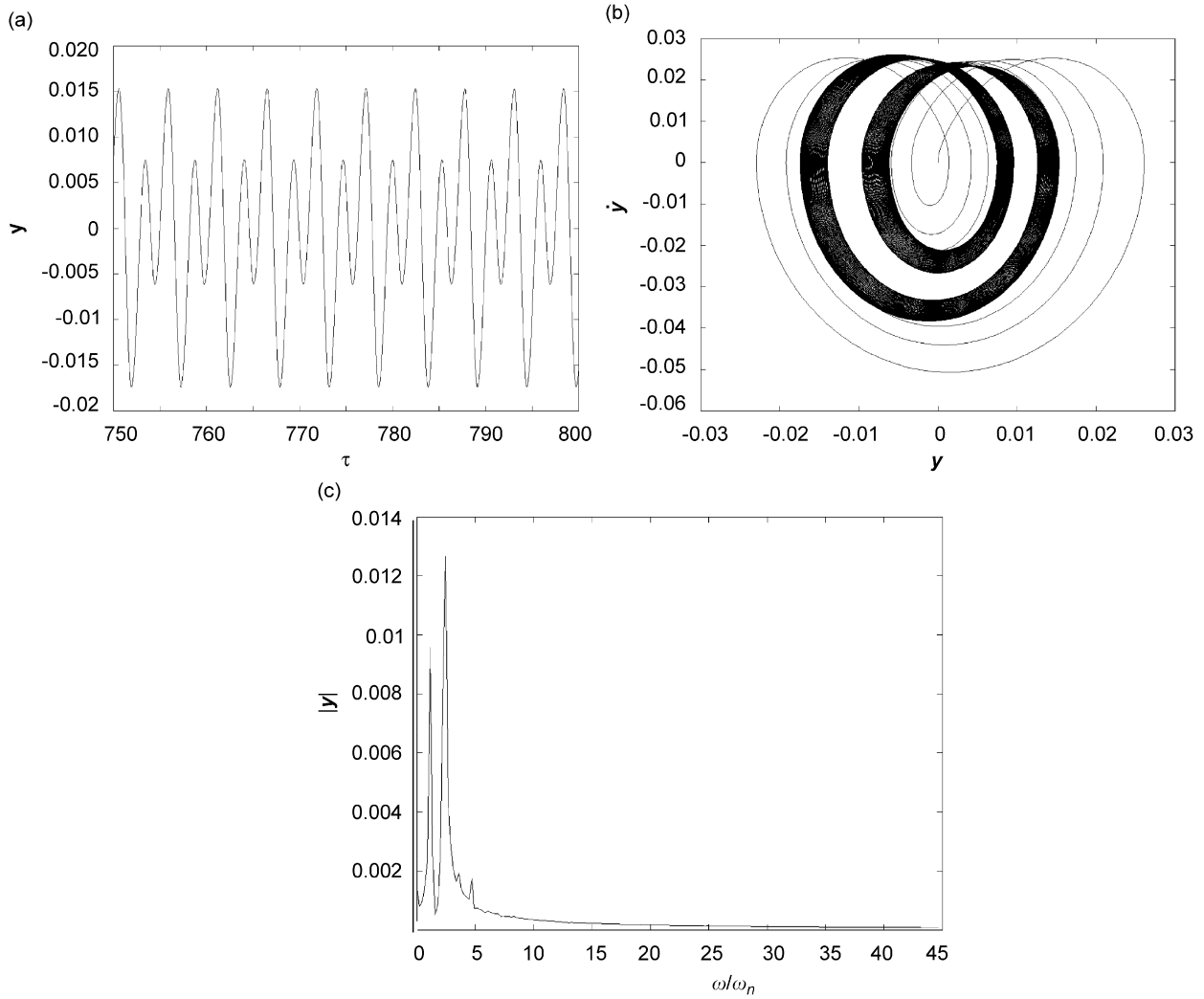

Fig. 8. (a) Response time history segment over 50 time unit window of frictional isolator showing multi-periodic non-harmonic response at excitation frequency $v = 2.3667$ and $f_o = 0.04$ $\mu_s = 0.5$ and $\mu_k = 0.3$, and (b) phase portrait, and (c) FFT plot.

$E[y^2]$ time histories are evaluated using the discrete formulas:

$$E[y] = \frac{1}{T}\int_0^T y(\tau)\,\mathrm{d}\tau \simeq \sum_{i=1}^{n}\frac{y_{ij}(\tau)}{n}, \quad j = 1,2,3,\ldots,N, \tag{34a}$$

$$E[y^2] = \frac{1}{T}\int_0^T y^2(\tau)\,\mathrm{d}\tau \simeq \sum_{i=1}^{n}\frac{y_{ij}^2(\tau)}{n}, \quad j = 1,2,3,\ldots,N, \tag{34b}$$

where n is the number of time points in each excitation record and N the total number of trials for each excitation intensity level. It is found that in order to achieve stationary response characteristics each time history should contain a sequence of $n = 38{,}400$ random numbers and each excitation is looped for $N = 300$ trials. The autocorrelation of the excitation and response time histories are evaluated using the MATLAB function *XCORR* and the PSD function using the routine *PWELCH*. The pdf is estimated using the *KSDENSITY* function.

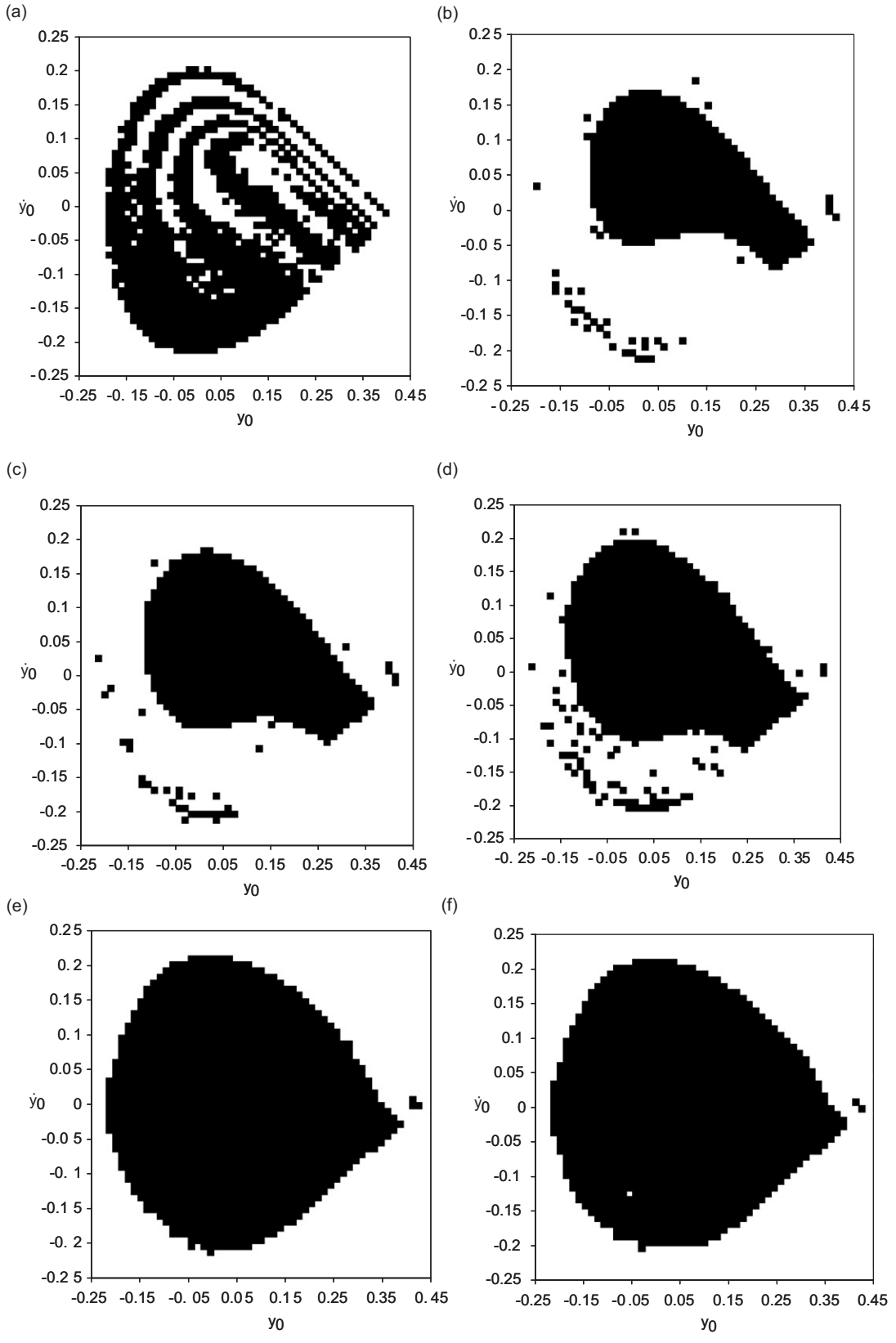

Fig. 9. Safe basins of attraction showing different response characteristics for different values of friction coefficient. $v = 0.85$ and $f_o = 0.0302$ ■: stable periodic non-harmonic response; empty space: unbounded (a) $\mu_k = 0.0$, (b) $\mu_k = 0.15$, (c) $\mu_k = 0.175$, (d) $\mu_k = 0.20$, (e) $\mu_k = 0.275$ (f) $\mu_k = 0.3$.

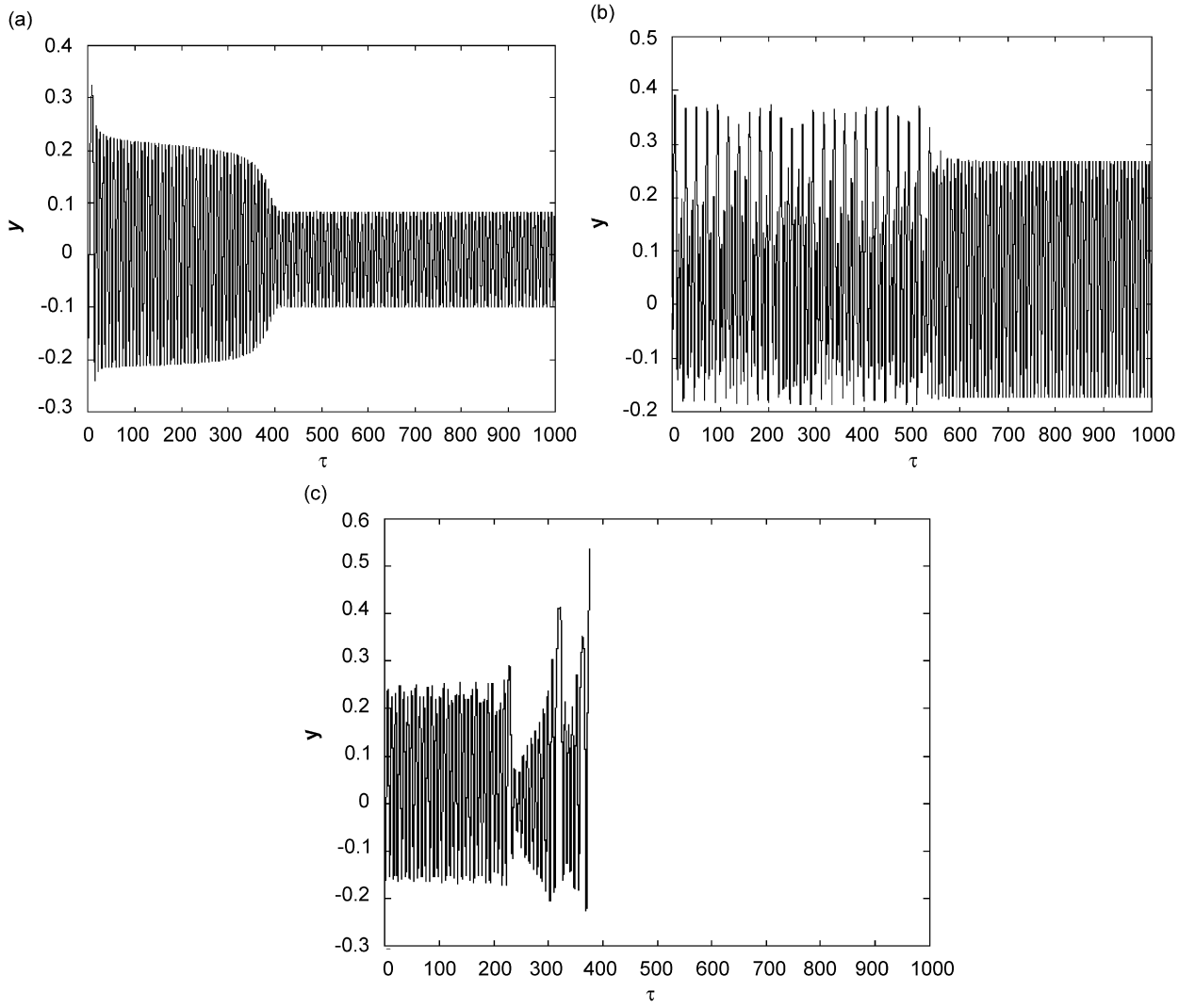

Fig. 10. Influence of initial conditions on the response time history record for $\mu_k = 0.3$, $v = 0.85$ and $f_o = 0.0329$: (a) $y_0 = -0.015$, $\dot{y}_0 = -0.1936$, (b) $y(0) = -0.106$; $\dot{y}(0) = 0.1584$, (c) $y(0) = -0.04$; $\dot{y}(0) = -0.1848$.

The Monte Carlo simulation is carried out for different values of excitation intensity level, $\pi S_o/2\zeta$. For each excitation intensity level the response is obtained for the frictionless beam and for the beam with the support friction coefficient $\mu_k = 0.3$. The response statistics for the excitation intensity level $\pi S_o/2\zeta = 0.0095$ are shown in Figs. 13(a)–(c). The PSD function shows a zero-mean mono-periodic response. The pdf shows a marked deviation from normality in the form of kurtosis. This characteristic is a reflection of the sporadic spikes in the time history response (not presented here) and is also accompanied by an elongation of the tails of the pdf. The mean square response time history shows higher initial oscillations at the outset of the simulation. This indicates that the friction has a destabilizing effect and the system requires a longer time to reach a stationary state. The mean square time history settles to a stationary value of 0.00629, which is lower than the frictionless level due to the friction dissipates energy and thus restrains the beam motion.

The excitation intensity $\pi S_o/2\zeta = 0.02366$ is identified as the limit based on the homoclinic orbit. The statistics of the response of this case are shown in Figs. 14(a)–(c) and demonstrate considerable nonlinear characteristics as indicated by the pdf. The level of kurtosis is indicative of the sporadic spikes in the time history record (not provided here). The mean square response stays consistently below the frictionless system

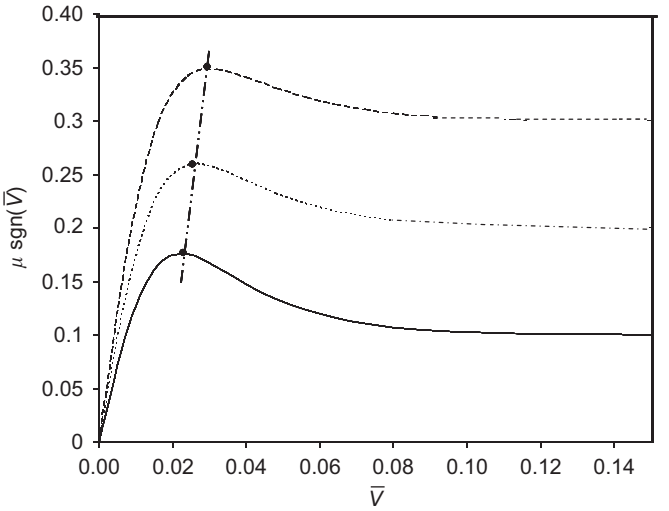

Fig. 11. Friction coefficient vs. relative velocity for three values of kinetic friction. _____ $\mu_k = 0.1$; - - - - - - - - - - - - - $\mu_k = 0.2$; - - - - - - - - - $\mu_k = 0.3$ ‥—●—‥ peak location.

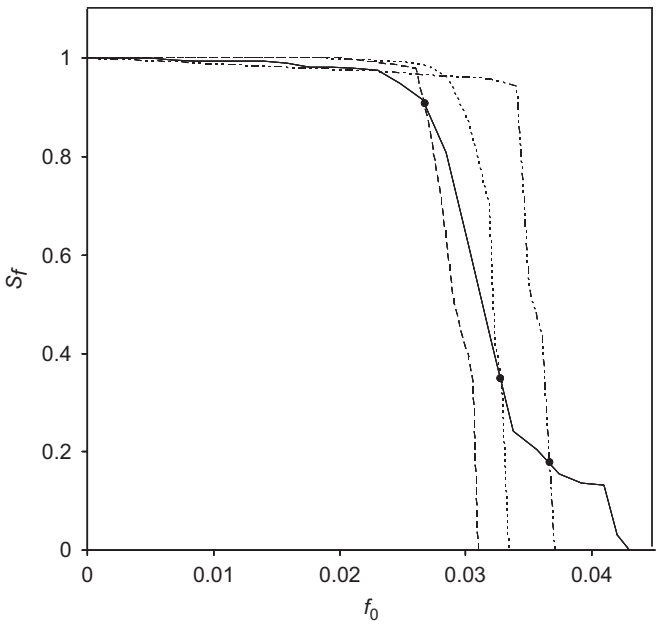

Fig. 12. Dependence of safety integrity factor on excitation amplitude level for three different values of friction coefficient. ——— $\mu_k = 0.0$; – – – – – $\mu_k = 0.1$; ▪▪▪▪▪▪▪▪▪▪▪▪ $\mu_k = 0.2$; ▬ · ▬ · ▬ · · $\mu_k = 0.3$ ●: crossing points.

response. The Monte Carlo simulations of both the frictionless and frictional isolator show non stationary responses for excitation levels beyond $\pi S_o/2\zeta = 0.02365$ which coincides with the maximum excitation level to maintain the homoclinic orbit of the unperturbed beam.

Fig. 15 shows the results of the Monte Carlo simulation presented as the dependence of the mean square response $E[y^2]$ on the excitation intensity, $\pi S_o/2\zeta$. The circles on the graph represent the responses obtained for the frictionless isolator and the squares for the frictional isolator with $\mu_k = 0.3$. Also, the closed-form solution for the frictionless isolator [46] is plotted in Fig. 15. The converged value of the mean square, $E[y^2]$,

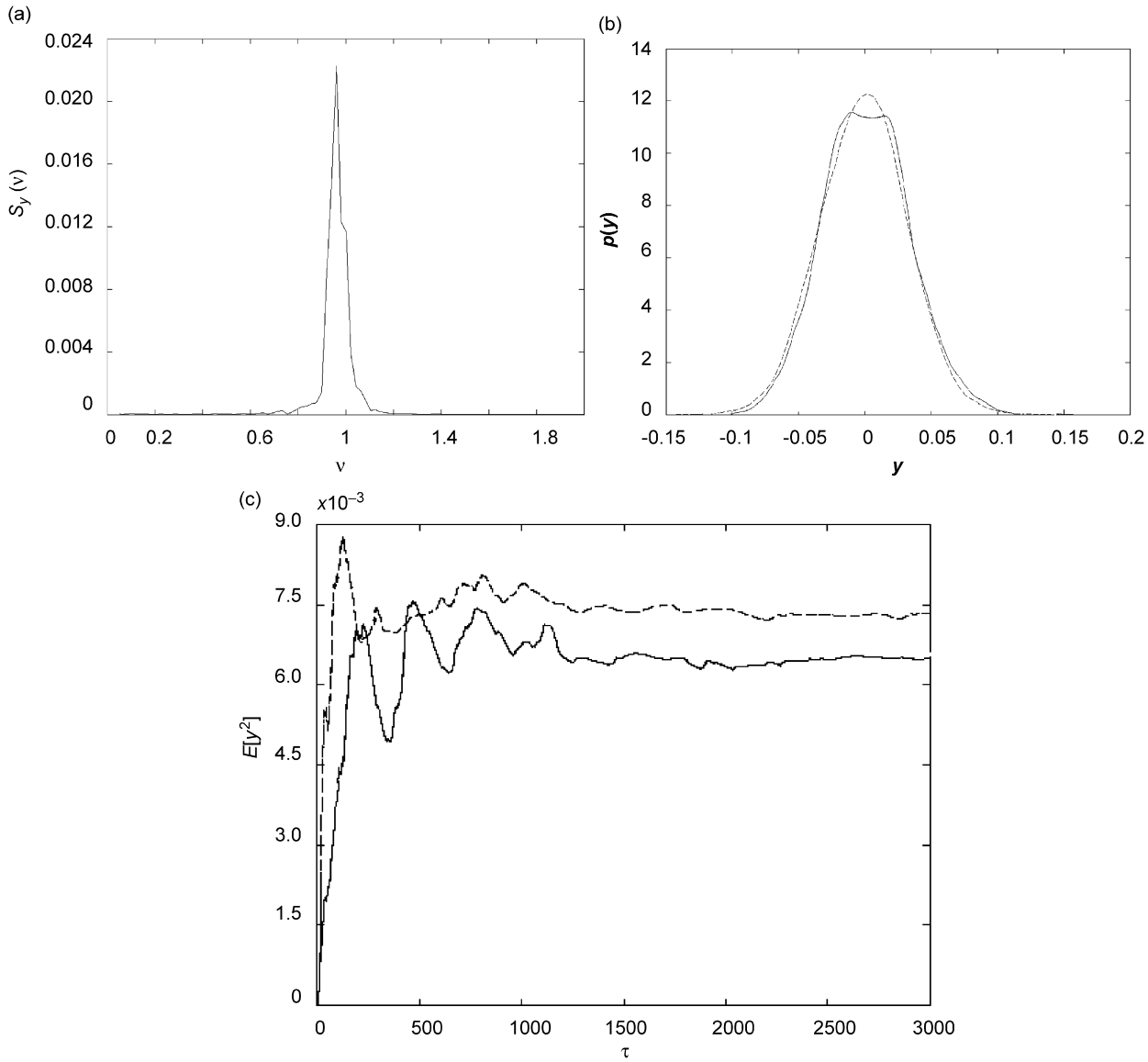

Fig. 13. Response statistics for $\pi S_o/2\zeta = 0.0095$, $\mu = 0.3$: (a) response power spectral density, (b) response probability density function, (c) mean square response time history: ————: $\mu_k = 0.3$, ------: $\mu_k = 0.0$.

closely matches the expected value of the total energy $E[H]$ of the closed-form solution [46]. They are related accordingly:

$$E[H] = E\left[V(y) + \frac{1}{2}\dot{y}^2\right] = E\left[\sum_{n=1}^{11} \frac{c_n y^{n+1}}{n+1} + \frac{1}{2}\dot{y}^2\right]$$
$$= E\left[\frac{1}{2}y^2 + \frac{1}{3}c_2 y^3 + \frac{1}{4}c_3 y^4 + \cdots + \frac{1}{2}\nu y^2\right] \simeq E[y^2](\because \nu = 1). \tag{35}$$

This equation indicates the approximate equivalence between the expected values of the mean square energy and the mean square response after neglecting the contribution of the higher-order terms to the mean square

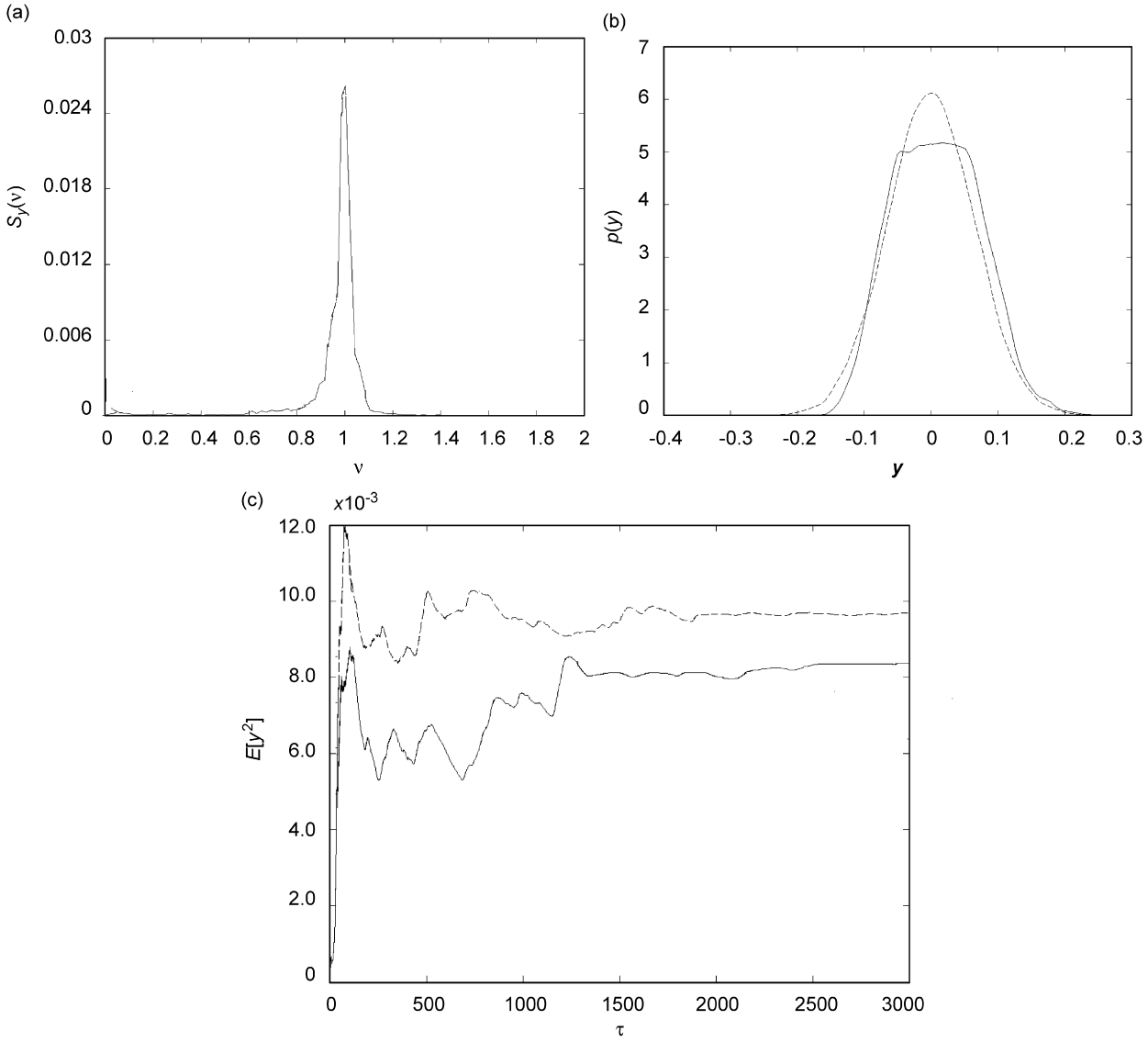

Fig. 14. Response statistics for $\pi S_o/2\zeta = 0.02365$, $\mu = 0.3$: (a) response power spectral density, (b) response probability density function, (c) mean square response time history: ——————: $\mu_k = 0.3$, ------: $\mu_k = 0.0$.

energy. The onset of nonlinearity in the response, which occurs at excitation intensity level $\pi S_o/2\zeta = 0.006$, is also indicated in both the closed form and simulation results.

6. Conclusions

The influence of friction due to beam sliding at its ends on its dynamic behavior and its efficacy as a nonlinear isolator has been studied numerically under sinusoidal and random excitation excitations. Under sinusoidal excitation, the equation of motion of the system is solved numerically and the solution is utilized to estimate the system transmissibility. It is found that when the excitation frequency is increased beyond resonance, the friction at the sliding supports serves to improve the transmissibility. The dependence of the safety integrity factor on excitation amplitude level and friction coefficient reveals that the friction extends the stable region. Under random excitation, the system response statistics were estimated from Monte Carlo

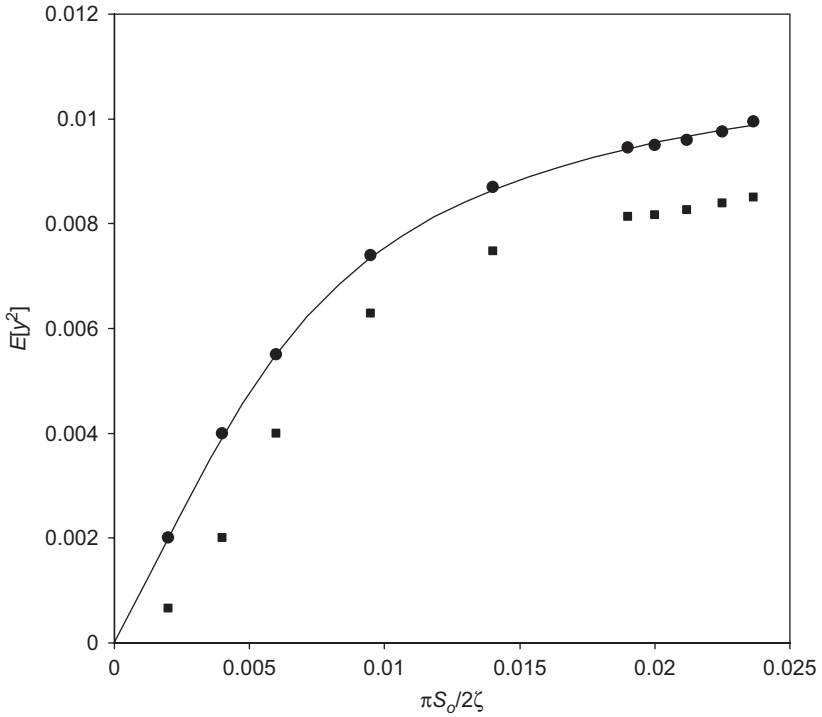

Fig. 15. Dependence of mean square response on excitation intensity level. ● ● ● ● ●: frictionless case ■ ■ ■ ■ ■: with friction $\mu_s = 0.5$; $\mu_k = 0.3$ ——————: analytical prediction in the absence of friction.

simulation results for different values of friction coefficient and excitation PSD level. The friction is found to result in a significant reduction of the system response mean square. The results of this work need to be validated experimentally and this task is currently underway.

Appendix A

$$c_2 = \frac{\tilde{S}(3a_3 + 10a_5\tilde{S}^2 + 21a_7\tilde{S}^4 + 36a_9\tilde{S}^6 + 55a_{11}\tilde{S}^8)}{(a_1 + 3a_3\tilde{S}^2 + 5a_5\tilde{S}^4 + 7a_7\tilde{S}^6 + 9a_9\tilde{S}^8 + 11a_{11}\tilde{S}^{10})},$$

$$c_3 = \frac{(a_3 + 10a_5\tilde{S}^2 + 35a_7\tilde{S}^4 + 84a_{11}\tilde{S}^6)}{(a_1 + 3a_3\tilde{S}^2 + 5a_5\tilde{S}^4 + 7a_7\tilde{S}^6 + 9a_9\tilde{S}^8 + 11a_{11}\tilde{S}^{10})},$$

$$c_4 = \frac{\tilde{S}(5a_5\tilde{S} + 35a_7\tilde{S}^2 + 126a_9\tilde{S}^4 + 330a_{11}\tilde{S}^6)}{(a_1 + 3a_3\tilde{S}^2 + 5a_5\tilde{S}^4 + 7a_7\tilde{S}^6 + 9a_9\tilde{S}^8 + 11a_{11}\tilde{S}^{10})},$$

$$c_5 = \frac{(a_5 + 21a_7\tilde{S}^2 + 126a_9\tilde{S}^4 + 462a_{11}\tilde{S}^6)}{(a_1 + 3a_3\tilde{S}^2 + 5a_5\tilde{S}^4 + 7a_7\tilde{S}^6 + 9a_9\tilde{S}^8 + 11a_{11}\tilde{S}^{10})},$$

$$c_6 = \frac{\tilde{S}(7a_7 + 84a_9\tilde{S}^2 + 462a_{11}\tilde{S}^4)}{(a_1 + 3a_3\tilde{S}^2 + 5a_5\tilde{S}^4 + 7a_7\tilde{S}^6 + 9a_9\tilde{S}^8 + 11a_{11}\tilde{S}^{10})},$$

$$c_7 = \frac{(a_7 + 36a_9\tilde{S}^2 + 330a_{11}\tilde{S}^4)}{(a_1 + 3a_3\tilde{S}^2 + 5a_5\tilde{S}^4 + 7a_7\tilde{S}^6 + 9a_9\tilde{S}^8 + 11a_{11}\tilde{S}^{10})},$$

$$c_8 = \frac{\tilde{S}(9a_9 + 165a_{11}\tilde{S}^3)}{(a_1 + 3a_3\tilde{S}^2 + 5a_5\tilde{S}^4 + 7a_7\tilde{S}^6 + 9a_9\tilde{S}^8 + 11a_{11}\tilde{S}^{10})},$$

$$c_9 = \frac{(a_9 + 55a_{11}\tilde{S}^2)}{(a_1 + 3a_3\tilde{S}^2 + 5a_5\tilde{S}^4 + 7a_7\tilde{S}^6 + 9a_9\tilde{S}^8 + 11a_{11}\tilde{S}^{10})},$$

$$c_{10} = \frac{11a_{11}\tilde{S}}{(a_1 + 3a_3\tilde{S}^2 + 5a_5\tilde{S}^4 + 7a_7\tilde{S}^6 + 9a_9\tilde{S}^8 + 11a_{11}\tilde{S}^{10})},$$

$$c_{11} = \frac{a_{11}}{(a_1 + 3a_3\tilde{S}^2 + 5a_5\tilde{S}^4 + 7a_7\tilde{S}^6 + 9a_9\tilde{S}^8 + 11a_{11}\tilde{S}^{10})}.$$

References

[1] M.Z. Kolovsky, *Nonlinear Dynamics of Active and Passive Systems of Vibration Protection*, Springer, Berlin, 1999.

[2] G.S. Yuryev, *Vibration Isolation of Precision Instruments*, Russian Academy of Sciences, Siberian Branch, Institute of Nuclear Physics Press, Novosibirsk, 1991 Reprint 89–146 (in Russian).

[3] J.P. DenHartog, Forced vibrations with constrained coulomb damping and viscous friction, *Transactions of the American Society of Mechanical Engineers* 53 (1931) 107–115.

[4] J.E. Ruzicka, T.F. Derby, *Influence of Damping in Vibration Isolation*, The Shock and Vibration Information Center, Washington, DC, 1971.

[5] M.S. Hundal, P.S. Parnes, Response of a base excitation system with Coulomb and viscous friction, *Journal of Sound and Vibration* 64 (1979) 371–378.

[6] S.M. Metwalli, Optimum nonlinear suspension system, *Proceedings of the American Society of Mechanical Engineers Technical Conference*, Vol. A4, Cincinnati, OH, 1985.

[7] B. Ravindra, A.K. Mallik, Performance of nonlinear vibration isolators under harmonic excitation, *Journal of Sound and Vibration* 170 (1994) 325–337.

[8] J.J. Lou, S.J. Zhu, L. He, X. Yu, Application of chaos method to line spectra reduction, *Journal of Sound and Vibration* 286 (2005) 645–652.

[9] A.M. Ulanov, G.V. Lazutkin, Description of an arbitrary multi-axial loading process for nonlinear vibration isolators, *Journal of Sound and Vibration* 203 (1997) 903–907.

[10] O. Qing, Z. Shi-Jian, S. Yin, A study of chaotic motion on nonlinear vibration–isolation system, *Proceedings of the 18th American Society of Mechanical Engineers Biennial Conference on Mechanical Vibration and Noise*, Pittsburgh, PA, Vol. 6C, September 9–12, 2001, pp. 2785–2787.

[11] P. Alabuzhev, A. Gritchin, L. Kim, G. Migirenko, V. Chon, P. Stepanov, *Vibration Protecting and Measuring Systems with Quasi-Zero Stiffness*, Hemisphere Publishing Co., Taylor & Francis Group, New York, 1989.

[12] V.P. Roslyakov, N.G. Nakhtigal, Choice of parameters of vibration protecting system with nonlinear characteristics, *Mechanization and Electrification of Agriculture* 10 (1975) 36–37.

[13] A.K. Zuyev, A.A. Nikitin, Vibration protecting mechanism for a riveting hammer, *Proceedings of Dynamics of Vibro-Impact Mechanical Systems*, *Novosibirsk, Novosibirsk Electro-Technical Institute (NETI)*, 1973, pp. 50–52.

[14] P. Alabuzhev, A. Gritchin, P.T. Stepanov, V.F. Khon, Studies of vibro-protecting systems with stiffness correction, *Physico-Technical Problems of Exploitation of Mineral Resources* 3 (1977) 136–149.

[15] P.T. Stepanov, Investigation of vibro-impact mechanical systems, *Novosibirsk, Novosibirsk Electro-Technical Institute (NETI)*, 1979, pp. 67–71.

[16] A.F. Yashin, L.I. Kim, I.S. Nikiforov, Nonlinear vibrations of systems with an arbitrary polynomial restoring force, *Proceedings of Mechanics of Deformed Bodies and Structural Calculations, Novosibirsk, Nauchnii Institut Zheleznodoro-zhnogo Transporta (Novosibirsk Institute of Railroad Transportation Engineers) (NIIZhT)*, 1975, pp. 136–143.

[17] I.I. Gerner, L.I. Kim, N.V. Mokin, Calculation of nonlinear corrector for vibration isolated suspension, *Proceedings of the Research for Railway Transportation, Nauchnii Institut Zheleznodoro-zhnogo Transporta (Novosibirsk Institute of Railroad Transportation Engineers) (NIZhT), Novosibirsk* No. 156, 1974, pp. 152–159.

[18] G.S. Yuryev, Computational analysis of a spring with quasi-zero stiffness, *Study of Vibro-Impact Mechanical Systems, Novosibirsk, Novosibirsk Electro-Technical Institute (NETI)*, 1979, pp. 84–90.

[19] V.N. Goverdovskiy, B.S. Gyzatullin, V.A. Petrov, Method of vibration isolation for the man-operator of transport-technological machine, Patent 2115570, Russia, 1998.
[20] C.M. Lee, V.N. Goverdovskiy, Alternative vibration protecting systems for men-operators of transport machines: modern level and prospects, *Journal of Sound and Vibration* 249 (2002) 635–647.
[21] C.M. Lee, V.N. Goverdovskiy, S.B. Samoilenko, Prediction of non-chaotic motion of the elastic system with small stiffness, *Journal of Sound and Vibration* 272 (2004) 643–655.
[22] R. Dufour, J. Der Hagopian, M. Pompei, C. Garnier, Shock and sine response of rigid structures on nonlinear mounts, *ASME Design Engineering Division (Publication), Structural Vibration and Acoustics* 34 (1991) 171–176.
[23] M.W. Dobry, J. Brzezinski, Vibro-isolation of pneumatic hammer, *Revue Francaise de Mecanique* 3 (1993) 439–444 (in French).
[24] D.V. Balandin, N.N. Bolotnik, W.D. Piley, Limiting performance analysis of impact isolation systems for injury prevention, *Shock and Vibration Digest* 33 (2001) 453–472.
[25] C. Zhiqing, W.D. Pilkey, Application of wavelets to optimal shock and impact isolation, *Transactions of Nanjing University of Aeronautics and Astronautics* 18 (2001) 1–10.
[26] A.M. Veprik, A. Meromi, A. Leschecz, Novel technique of vibration control for split Sterling crycooler with linear compressor, *Proceedings of the International Society for Optical Engineering (SPIE) 11th Annual International Symposium on Aerospace/Defense Sensing, Simulation and Controls AeroSense, Orlando, FL, Vol. 3061: Infrared Technology and Applications* XXIII, 1997, pp. 640.
[27] V.I. Babitsky, *Theory of Vibro-Impact Systems with Applications*, Springer, Berlin, 1998.
[28] V.I. Babitsky, A.M. Veprik, Universal bumpered vibration isolator for severe environment, *Journal of Sound and Vibration* 218 (1998) 269–292.
[29] D.G. Blair, F.J. van Kann, A.L. Fairhall, Behavior of a vibration isolator suitable for use in cryogenic or vacuum environments, *Measurement Science and Technology* 2 (1991) 846–850.
[30] L. Ju, D.G. Blair, Low resonant frequency cantilever spring isolator for gravitational wave detectors, *Review of Scientific Instruments* 65 (1994) 3482–3488.
[31] G. Losurdo, M. Bernardini, S. Braccini, C. Bradaschia, C. Casciano, V. Dattilo, R. DeSalvo, A. DiVirgilio, F. Frasconi, A. Gaddi, A. Gennai, A. Giazotto, H.P. Pan, F. Paoletti, A. Pasqualetti, R. Passaquieti, D. Passuello, R. Taddei, Z. Zhang, G. Cella, E. Cuoco, E. D'Ambrosio, F. Fidecaro, S. Gaggero, P. LaPenna, S. Mancini, R. Poggiani, A. Vicerè, M. Mazzoni, R. Stanga, L. Holloway, J. Winterflood, An inverted pendulum pre-isolator stage for the VIRGO suspension system, *Review of Scientific Instruments* 70 (1999) 2507–2515.
[32] M.V. Plissi, C.I. Torrie, M.E. Husman, N.A. Robertson, K.A. Strain, H. Ward, H. Lück, J. Hough, GEO 600 triple pendulum suspension system: seismic isolation and control, *Review of Scientific Instruments* 71 (2000) 2539–2545.
[33] G. Ballardin, L. Bracci, S. Braccini, C. Bradaschia, C. Casciano, G. Calamai, R. Cavalieri, R. Cecchi, G. Cella, E. Cuoco, E. D'Ambrosio, V. Dattilo, A. DiVirgilio, L. Fabbroni, F. Fidecaro, F. Frasconi, A. Gaddi, A. Gennai, A. Giazotto, G. Losurdo, L. Holloway, P. LaPenna, F. Lelli, E. Majorana, M. Mazzoni, F. Paoletti, M. Pasotti, A. Pasqualetti, R. Passaquieti, D. Passuello, R. Poggiani, P. Puppo, F. Rafaelli, P. Rapagnani, F. Ricci, R. Ruggi, R. Stanga, R. Taddei, F. Vetrano, A. Vicerè, Z. Zhang, Measurement of the VIGRO super-attenuator performance for seismic noise suppression, *Review of Scientific Instruments* 72 (2001) 3643–3652.
[34] R. Takahashi, F. Kuwahara, E. Majorana, M.A. Barton, T. Uchiyama, K. Kuroda, A. Araya, K. Arai, A. Takamori, M. Ando, K. Tsubono, M. Fukushima, Y. Saito, Vacuum-compatible vibration isolation stack for an interferometric gravitational wave detector TAMA300, *Review of Scientific Instrument* 73 (2002) 2428–2433.
[35] R. Takahashi, K. Arai, Improvement of the vibration isolation system for TAMA300, *Classical and Quantum Gravity* 19 (2002) 1599–1604.
[36] J. Winterflood, D.G. Blair, B. Slagmolen, High performance vibration isolation using springs in Euler column buckling mode, *Physics Letters A* 300 (2002) 122–130.
[37] J. Winterflood, T.A. Barber, D.G. Blair, Mathematical analysis of an Euler spring vibration isolator, *Physics Letters A* 300 (2002) 131–139.
[38] L.N. Virgin, R.B. Davis, Vibration isolation using buckled structures, *Journal of Sound and Structures* 260 (2003) 965–973.
[39] R.H. Plaut, J.E. Sidbury, L.N. Virgin, Analysis of buckled and pre-bent fixed-end columns used as vibration isolators, *Journal of Sound and Vibration* 283 (2005) 1216–1228.
[40] R.H. Plaut, L.A. Alloway, L.N. Virgin, Nonlinear oscillations of a buckled mechanism used as a vibration isolator, in: G. Rega, F. Vestroni (Eds.), *Proceedings of the IUTAM Symposium on Chaotic Dynamics and Control of Systems and Processes in Mechanics*, Springer, The Netherlands, 2005, pp. 241–250.
[41] T.E. Shoup, Shock and vibration isolation using a nonlinear elastic suspension, *American Institute of Aeronautics and Astronautics Journal* 9 (1971) 1643–1645.
[42] T.E. Shoup, G.E. Simmonds, An adjustable spring rate suspension system, *American Institute of Aeronautics and Astronautics Journal* 15 (1977) 865–866.
[43] R.A. Ibrahim, Recent advances in nonlinear vibration isolators, *Journal of Sound and Vibration* (under review).
[44] D. Kisliakov, Dynamic analysis of a multiple-supported pressure pipeline subjected to both axial and vertical seismic excitation components, *Proceedings of the Third International Conference on Seismology and Earthquake Engineering*, Vol. II, Iran, 1999, pp. 881–898.
[45] D. Kisliakov, Axial earthquake-induced vibrations of a pressure pipeline on frictional support columns, *Proceedings of the Anniversary Scientific Conference on 50 years Faculty of Hydraulic Engineering at UACEG*, Vol. III, Sofia, 1999.

[46] R. Somnay, R.A. Ibrahim, R.C. Banasik, Nonlinear dynamics of a sliding beam on two supports and its efficacy as a non-traditional isolator, *Journal of Vibration and Control* 12 (2006) 685–712.
[47] D. Gospodnetic, Deflection curve of a simply supported beam, *Journal of Applied Mechanics—Transactions of the ASME* 26 (1959) 675–676.
[48] R. Frisch-Fay, *Flexible Bars*, Butterworths, London, 1962.
[49] B.F. Feeny, F.C. Moon, Autocorrelation on symbol dynamics with dry friction oscillator, *Physics Letters A* 141 (1989) 397–400.
[50] A. Filippov, *Differential Equations with Discontinuous Right-Hand Sides*, American Mathematical Society Translation 42, Series 2, Providence, RI, 1964.
[51] J.R. Dormand, P.J. Prince, A family of embedded Runge–Kutta formulae, *Journal Computational and Applied Mathematics* 6 (1980) 19–26.
[52] G. Marsaglia, W.W. Tsang, The Ziggurat method for generating random variables, *Journal of Statistical Software* 5 (2000). Available online at 〈http://www.jstatsoft.org/v05/i08/〉.